

Lightweight LiDAR-Camera 3D Dynamic Object Detection and Multi-Class Trajectory Prediction

Yushen He¹, Lei Zhao¹, Tianchen Deng¹, Zipeng Fang¹, and Weidong Chen^{1*}, *Member, IEEE*

Abstract—Service mobile robots are often required to avoid dynamic objects while performing their tasks, but they usually have only limited computational resources. So we present a lightweight multi-modal framework for 3D object detection and trajectory prediction. Our system synergistically integrates LiDAR and camera inputs to achieve real-time perception of pedestrians, vehicles, and riders in 3D space. The framework proposes two novel modules: 1) a Cross-Modal Deformable Transformer (CMDT) for object detection with high accuracy and acceptable amount of computation, and 2) a Reference Trajectory-based Multi-Class Transformer (RTMCT) for efficient and diverse trajectory prediction of multi-class objects with flexible trajectory lengths. Evaluations on the CODa benchmark demonstrate superior performance over existing methods across detection (+2.03% in mAP) and trajectory prediction (-0.408m in minADE₅ of pedestrians) metrics. Remarkably, the system exhibits exceptional deployability - when implemented on a wheelchair robot with an entry-level NVIDIA 3060 GPU, it achieves real-time inference at 13.2 fps. To facilitate reproducibility and practical deployment, we release the related code of the method at https://github.com/TossherO/3D_Perception and its ROS inference version at https://github.com/TossherO/ros_packages.

I. INTRODUCTION

Safe autonomous navigation for service mobile robots in daily life scenarios fundamentally relies on robust 3D scene reconstruction [1], [2] and perception of dynamic objects such as pedestrians, vehicles, riders, etc. Existing works usually use an end-to-end model or a sequential model of detection, tracking, and trajectory prediction to realize the perception tasks. While end-to-end models demonstrate competitive performance, their computational complexity and scene-specific optimization (typically for autonomous driving [3], [4]) render them impractical for resource-limited mobile robots operating across diverse daily environments. In contrast, modular sequential frameworks enable real-time deployment through hardware-aware component optimization, better aligning with mobile robots' operational constraints. The subsequent discussion will be organized into three key components: object detection, object tracking, and trajectory prediction.

For detection task, LiDAR-camera fused models [5]–[7] tend to be high performing, but complicated in structure. The query-based detection models [8], [9] have a flexible structure that is better for detecting objects with different scales and distributions. CMT [10] extends the query-based detection method to multi-modal network with a simple architecture, but

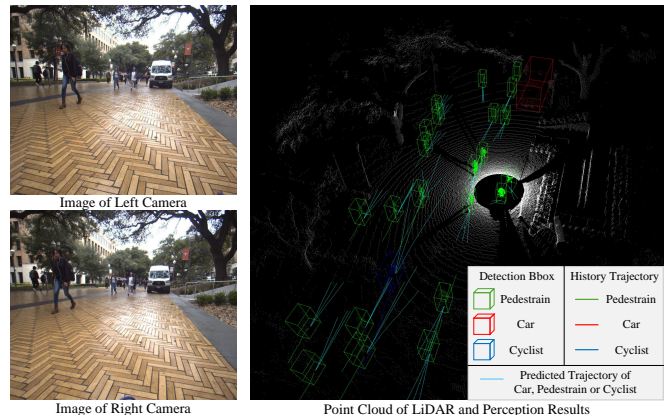


Fig. 1: Detection and trajectory prediction results of our method on CODa.

it uses global attention that has high computational overhead, and its accuracy can be improved.

For tracking task, the TBD method SimpleTrack [11] is lightweight for mobile robot platforms and can achieve great tracking performance. However, it infers on the CPU, which inference speed can be further improved with the parallel acceleration of GPU.

For trajectory prediction task, some works [12]–[14] are applied to autonomous driving scenes, which require maps prior and focus on modeling elements such as lanes. They are not fit for mobile robots in scenes of daily life. Other works [15]–[22] predict trajectories of pedestrians which take fixed-length trajectories as input and can not predict trajectories for multiple classes of objects with flexible trajectory lengths.

According to above problems, considering the needs of safely autonomous navigation in scenes of daily life, we use LiDAR and cameras as sensors to design a lightweight perception model for service mobile robots to perform real-time detection, tracking and trajectory prediction of multiple classes of dynamic objects such as pedestrians, vehicles and riders in 3D scenes. We open-sourced related models and deployment approaches to benefit the robotics community.

Our contributions are mainly as follows:

- We propose a lightweight multi-modal framework for 3D object detection and trajectory prediction, which consists of our detection model, our trajectory prediction model, and improved SimpleTrack as a tracking model.
- We propose the LiDAR-camera fused detection model Cross Model Deformable Transformer (CMDT). Introduce the 3D Multi-Model Deformable Attention

*The corresponding author, wdchen@sjtu.edu.cn.

¹Institute of Medical Robotics and Department of Automation, Shanghai Jiao Tong University, Key Laboratory of System Control and Information Processing, Ministry of Education, Shanghai 200240, China.

(MMDA) module in its transformer and improve training strategies to effectively increase the detection accuracy of objects at different scales while reducing the amount of computation.

- We propose the trajectory prediction model Reference Trajectory based Multi-Class Transformer (RTMCT). It can predict trajectories for multiple classes of objects with flexible trajectory lengths by reference trajectories and transformer, while achieving high computational efficiency and diversity of predicted trajectories.
- On pedestrian dataset CODa [23], our method outperforms many representative methods. Fig. 1 shows its results on CODa. Also, by collecting a little data (861 frames of samples) for training, the method can be applied on a resource-constrained mobile robot platform to achieve real-time inference with fine accuracy.

II. RELATED WORK

A. 3D Object Detection

Earlier 3D object detection methods [24]–[27] mainly use LiDAR as the sensor. With the proposal of LSS [28], the use of cameras has become popular, both the methods using monocular [29] and multi-view [30]–[32] cameras achieve effective improvement in accuracy. In addition, with the proposal of DETR [33], query-based detection methods begin to develop, from 2D detection methods [34]–[36] to camera-based 3D detection methods [8], [9].

Compared to using a single-sensor method, combining the advantages of LiDAR in geometric information and the camera in semantic information can achieve higher accuracy. In early fusion work, the performance improvement was not significant due to limitations in network structure or fusion strategies. MVXNet [37] starts to use voxel-based approach to fuse point cloud and image features by Point-Fusion or Voxel-Fusion ways. Afterward, researchers started to try more efficient fusion methods, BEVFusion [7] transforms the image features by LSS, and achieves feature-level fusion in BEV. Based on PETR [9], CMT [10] extends the this framework to multi-modal network. Although CMT has a simple architecture, its queries interact with all image and point cloud features by global cross attention in transformer. It has a large amount of computation and memory consumption, and an accuracy that can be improved.

B. Object Tracking

According to the framework of object tracking methods, they can be decomposed into three categories: 1) the Tracking by Detection (TBD) framework; 2) the Joint Detection and Tracking (JDT) framework; 3) the Tracking by Attention (TBA) framework. The TBD framework mainly uses the detection results from other methods as input for tracking. SORT [38] tracks objects in 2D images by Kalman filtering and Hungarian matching algorithm. AB3DMOT [39] extends the TBD tracking framework to 3D scenes, and then improved methods [11], [40]–[42] have been proposed. For the JDT framework, some methods [43], [44] get tracking-related information while performing the detection. Based on

Deformable DETR [34], TransTrack [45] extends the query-based object detection method to an end-to-end detection and tracking method in 2D scenes, creating the Tracking-by-Attention (TBA) framework. Some works use this framework for 2D scenes [46], [47] and 3D scenes [48]–[50].

Although the JDT and TBA methods introduce more information in tracking, their models are complicated, difficult to train, and hard to transfer across different application scenes. TBD methods require no training, have fast speed and high accuracy, and are easy to adjust the parameters for different scenes. So TBD methods are still the optimal choice for practice.

C. Trajectory Prediction

Trajectory prediction methods are originally used to predict the trajectories of pedestrians. Social-LSTM [15] is the first to achieve reliable trajectory prediction of pedestrians with LSTM. There are also some other methods that use other networks, such as STGAT [16] uses graph network and graph attention and STAR [17] uses temporal transformer and spatial transformer, etc. But these methods are difficult to generate diverse trajectory predictions. In order to incorporate the uncertainty of pedestrians’ motions, some methods obtain diverse trajectory predictions by generative models. Methods [18]–[20] use Conditional Variational Auto-Encoder (CVAE), and methods [21], [22] use Generative Adversarial Networks (GANs). However, generative models tend to have complicated architectures and slower speeds, and are often difficult to train.

In addition to pedestrian trajectory prediction, many methods [12]–[14] are used for autonomous driving scenes. These methods usually require a known map and modeling of roads and lane lines to predict the trajectories of the vehicles. For mobile service robots targeting daily life scenarios, these methods may not be very suitable. We need to design a prediction framework for it that is oriented towards daily life scenarios.

III. METHOD

A. Overview

Our method consists of detection model, tracking model and trajectory prediction model. Refer to CMT [10], we propose a detection framework named Cross Model Deformable Transformer (CMDT) that integrates two key points for object detection. Specifically, we incorporate a 3D Multi-Modal Deformable Attention (MMDA) module into the transformer architecture, while simultaneously improving the model’s training strategy. They are presented in III-B. For tracking model, we choose SimpleTrack [11] and implement its main computation part on the GPU rather than CPU, which is presented in III-C. For trajectory prediction model, we propose Reference Trajectory based Multi-Class Transformer (RTMCT). It can predict trajectories for multiple classes of objects with flexible trajectory lengths, which is presented in III-D.

B. Detection Model

The architecture of CMDT is shown in Fig. 2. The image feature maps and the BEV’s point cloud feature map are

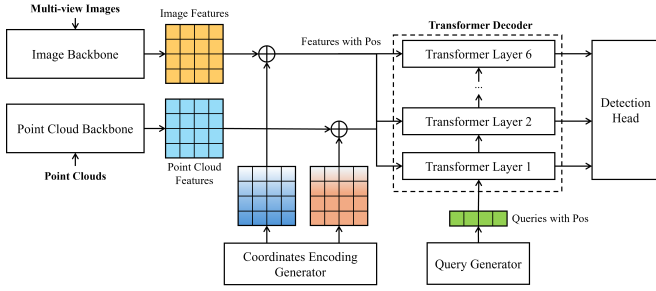


Fig. 2: Architecture of CMDT

obtained by the respective backbone. Coordinates Encoding Generator module generates positional coding with the same shape and dimension as the image and point cloud features. Query Generator module generates queries distributed in 3D space with their positional encoding. Coordinates Encoding Generator and Query Generator modules are the same as in CMT. Transformer Decoder contains 6 decoder layers, each layer consists of self-attention, cross-attention and FFN. The self-attention is a regular attention that enables interaction between queries. Different from CMT, cross-attention is MMDA module rather than regular attention, in which queries interact with the image and point cloud features around their positions. The results of the multiple decoder layers are passed through the same detection head to predict layer-by-layer optimized 3D bounding boxes and classes.

1) *3D Multi-Model Deformable Attention (MMDA)*: Referring to Deformable Attention [34], we design the MMDA module. Its structure is shown in Fig. 3. Let M be the number of attention heads, J be the number of cameras, and K be the number of sampling points. Let an input query be Q and its 3D reference point be p . Then the k -th 3D sampling point of the m -th head $p_{m,k}$ can be calculated by Eq. 1, where φ is a linear layer that outputs the 3D offsets.

$$p_{m,k} = \varphi_{m,k}(Q) + p \quad (1)$$

Each sampling point has a weight on each feature map. The weights on the point cloud feature map are obtained directly from Q through a linear layer and softmax operation, while the weights on the image feature maps need to be additionally encoded by camera parameters to discriminate different images. Let E_j be the intrinsic and extrinsic parameters of the j -th camera, then the weight of the sampling point of the m -th head on the j -th image can be calculated by Eq. 2, where ψ is a linear layer with softmax.

$$A_m^{I,j} = \psi_m^{I,j} [Q + MLP(E_j)] \quad (2)$$

Let $p_{m,k}^{Pc}$ and $p_{m,k}^{I,j}$ be the positions of $p_{m,k}$ projected on the point cloud feature map and the j -th image feature map. $Pc(x)$ and $Im_j(x)$ refer to feature vectors obtained via bilinear interpolation of the position x , respectively, on the point cloud feature map and the j -th image feature map. Then the point cloud and image values can be calculated by Eq. 3 and Eq. 4, respectively.

$$V_{Pc} = \sum_{m=1}^M W_m^{Pc} \left[\sum_{k=1}^K A_{m,k}^{Pc} \cdot Pc(p_{m,k}^{Pc}) \right] \quad (3)$$

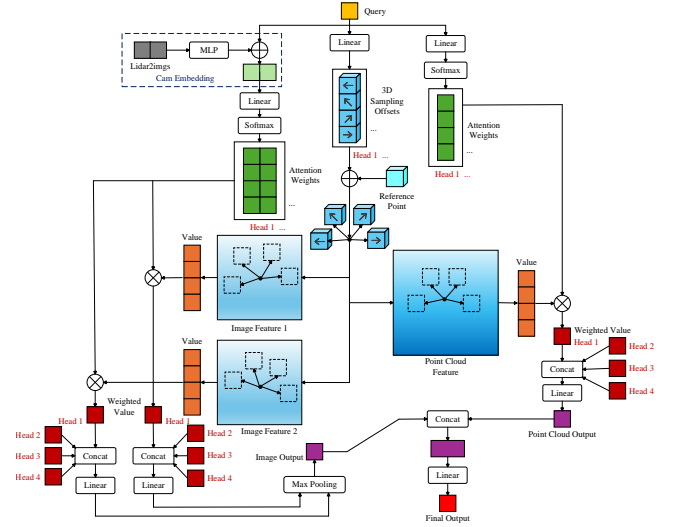


Fig. 3: Architecture of MMDA module

$$V_{Im,j} = \sum_{m=1}^M W_m^{Im,j} \left[\sum_{k=1}^K A_{m,k}^{Im,j} Im_j(p_{m,k}^{Im,j}) \right] \quad (4)$$

Finally, multiple image values through max pooling are concatenated with the point cloud value, then through a linear layer to get the final output, as in Eq. 5.

$$V_{out} = W_{out} \cdot Concat(max_j\{V_{Im,j}\}, V_{Pc}) \quad (5)$$

In MMDA module, queries only sample key information from the image and point cloud features according to the position and class of the object they detect. This reduces the computation and also benefits the network to learn more meaningful information.

2) *Improvements of Training Strategies*: The training loss includes focal loss for classification and L1 loss for 3D bounding box regression. In CMT, the results of each layer of decoder are taken into the loss calculation with the same weight. However, we want to get layer-by-layer optimized 3D bounding box predictions. If the former layers of decoder are trained with the goal of accurate prediction, it will increase the training difficulty. So we propose a regression loss that becomes stricter layer by layer, called the 3D bounding box truncated L1 loss. For a layer of decoder, given a truncation threshold τ , a bounding box prediction $DT = [x', y', z', l', w', h', \theta']^T$ and a ground truth $GT = [x, y, z, l, w, h, \theta]^T$, the loss is computed as shown in Eq. 6, where c is a weight vector.

$$Loss = c^T \cdot max \left(|GT - DT| - [l\tau, w\tau, h\tau, l\tau, w\tau, h\tau, \tau]^T, 0 \right) \quad (6)$$

In addition, the model employs the denoising strategy [35] to accelerate convergence. However, in the later part of training, the auxiliary task introduced by the denoising strategy may slightly hinder the model's convergence to higher accuracy. Thus, we choose to terminate the denoising strategy early during training.

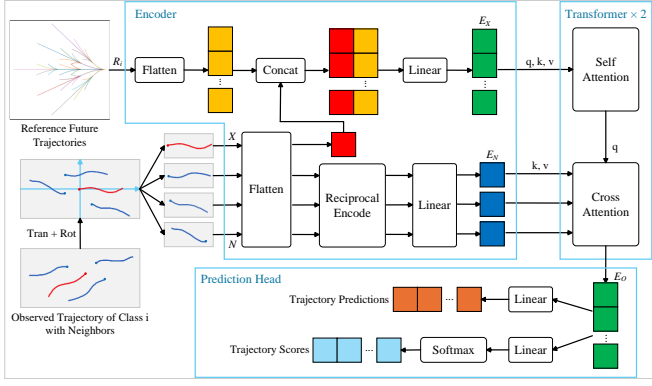


Fig. 4: Architecture of RTMCT

C. Tracking Model

SimpleTrack [11] generally meets our need for a high-precision and lightweight model, so we choose it as our tracking model. SimpleTrack infers on the CPU. Its main computation part is the association matrix between tracklets and detections, which uses 3D GIOU as the matching metric. However, 3D GIOU involves the complex calculation of the enclosing convex between two 3D bounding boxes, and it is a volume-only metric. So we replaced 3D GIOU with 3D DIOU as the metric. 3D DIOU combines distance and volume metrics, which is more advantageous when facing dynamic objects with unstable 3D dimensions of bounding boxes, and it avoids the calculation of the enclosing convex. We further implement the computation of the association matrix on the GPU, greatly increasing the inference speed.

D. Trajectory Prediction Model

The architecture of RTMCT is shown in Fig. 4. RTMCT inputs BEV’s trajectories of multi-class objects and the robot itself with flexible lengths, and outputs predicted trajectories of these objects. Instead of using generative models such as CVAE, or GANs, we only use linear layers and transformer to encode and decode trajectories in parallel and consider the interactions of different objects. The diverse trajectory predictions are efficiently generated by reference future trajectories. We present the model in several parts: trajectories preprocessing, reference future trajectories generation, trajectories encoding, transformer decoding, prediction head and loss.

1) *Trajectory Preprocessing:* The model takes each observed trajectory with its neighbors as an input. Let T_{obs} be the length of input trajectory, and T_{min} be the minimum length of observed trajectory. When the length of a trajectory is less than T_{min} , it is padded with the earliest position of trajectory to reach T_{obs} . Neighbors are selected based on their distance from the observed trajectory. Let c be the number of classes, and set the distance thresholds d_1, \dots, d_{c+1} depending on the influence range of each class (the robot itself is additionally treated as a class). Let the class of the current observed trajectory be i . If the minimum distance between current trajectory and a trajectory of class j is less than $\max(d_i, d_j)$, this trajectory is included in neighbors. A neighbor trajectory may have positions missing within the length of T_{obs} , in which case

the missing $[x, y]$ positions are filled with extremely large values. Then we obtain a observed trajectory $X \in \mathbb{R}^{T_{obs} \times 2}$, and its neighbors $N \in \mathbb{R}^{k \times T_{obs} \times 2}$, with k being the number of neighbors. To facilitate model processing, we apply translation and rotation to the observed trajectories and their neighbors so that the last position of the observed trajectory is located at the origin and the earliest position is located on the positive X-axis. Thus all input observed trajectories have similar positions and orientations.

2) *Reference Future Trajectory Generation:* Let T_{pred} be the length of the predicted trajectory and n be the number of reference trajectories. A set of reference trajectories $R \in \mathbb{R}^{c \times n \times T_{pred} \times 2}$ will be generated before training, with their positions as learnable parameters, where n is also the number of predicted future trajectories for each observed trajectory. To generate reference trajectories, we set m motion modes, each including a linear velocity and an angular velocity. Then a reference trajectory is equally divided into two parts, each part taking one of the m motion modes, thus generating reference trajectories with a total number of $n = m^2$. Due to their learnability, these reference trajectories will adjust to the appropriately distributed during training.

3) *Trajectory Encoding:* Firstly, the observed trajectory X with class i , its neighbors N , and its corresponding reference trajectories $R_i \in \mathbb{R}^{n \times T_{pred} \times 2}$, are flattened to get $X' \in \mathbb{R}^{2T_{obs}}$, $N' \in \mathbb{R}^{k \times 2T_{obs}}$, and $R'_i \in \mathbb{R}^{n \times 2T_{pred}}$. For observed trajectory X' , it is concatenated with each R'_i , and passes through a linear layer ϕ_i (for c classes, there exists linear layers ϕ_1, \dots, ϕ_c) to obtain the encoded self-trajectory $E_X \in \mathbb{R}^{n \times d}$, where d is the embedding dimension. For the neighbors N' , since the closer they are to the current position of observed trajectory (i.e., the origin), the more they have effects on it, we take the reciprocal number for them. Taking the reciprocal also transforms the extremely large values filled in the neighbors into tiny values, avoiding abnormal training of the network. Then for each neighbor, if it is of class j , it is encoded through a linear layer ψ_j . Since there are $c + 1$ classes of neighbors containing the robot itself, there exist linear layers $\psi_1, \dots, \psi_{c+1}$. The encoded results for all neighbors compose $E_N \in \mathbb{R}^{k \times d}$.

4) *Transformer Decoding:* The transformer decoder has 2 decoder layers, each consisting of self-attention, cross-attention and FFN. Both the self-attention and cross-attention are regular attentions. The self-trajectory E_X is input to the transformer decoder as initial queries. In self-attention, queries with different reference trajectories interact with each other, to compare which prediction of query is more likely to be realistic. In cross-attention, the self-trajectory interacts with neighbors to adjust its predictions. $E_O \in \mathbb{R}^{n \times d}$ is the output of the transformer decoder.

5) *Prediction Head and Loss:* The prediction head takes E_O as input and contains two branches, the trajectory prediction head and the score head. The trajectory prediction head is a linear layer that outputs future trajectory predictions $Y' \in \mathbb{R}^{n \times T_{pred} \times 2}$, and the score head is a linear layer with softmax that outputs confidence scores for each prediction. Different linear layers are used for different classes of objects.



Fig. 5: Mobile robot platform.

TABLE I: Performance of detection models on CODa

Methods	Modality	AP(Pedestrian)	AP(Car)	AP(Cyclist)	mAP
CenterPoint [26]	L	75.56	52.56	60.64	62.92
BEVFusion [7]	L+C	79.55	54.18	63.74	65.82
CMT [10]	L+C	80.87	62.41	66.38	69.89
CMDT(ours)	L+C	81.15	65.24	69.38	71.92

In training, given a real future trajectory $Y \in \mathbb{R}^{T_{pred} \times 2}$, the Average Displacement Error (ADE) between Y and each of n reference future trajectories R_i is computed respectively. Then the output associated with the reference trajectory that have the smallest ADE is selected as the positive sample as shown in Eq. 7. The loss function includes trajectory prediction loss and score loss. The trajectory prediction loss is Smooth L1 loss between positive sample Y'_t and Y , and the score loss is cross-entropy loss for the positive sample with truth value 1.

$$t = \underset{t \in \{1, \dots, n\}}{\operatorname{argmin}} \|Y - R_{i,t}\|_2 \quad (7)$$

IV. EXPERIMENTS

We use a public dataset to test the performance of our method on detection, tracking, and trajectory prediction tasks. Then we use a mobile robot platform to test the deployability of our method. Additional ablation experiments are conducted to verify the effectiveness of the proposed components.

Dataset: Dataset CODa [23] is used for experiments. It is collected in a campus environment with a mobile robot as the perception subject, covering both indoor and outdoor scenes with different lighting and weather conditions, containing labels of 53 classes for 3D object detection. The data collection rate is 10 fps. We use the data collected by a 128-line LiDAR and two RGB cameras, and split it into train, validation, and test sets with lengths of 18050, 4906, and 4907. We perceive only dynamic objects and use the same labels Pedestrian, Car, and Cyclist as in KITTI [51], where all vehicle-related classes in the CODa dataset are unified as Car, and classes Bike, Motorcycle, and so on are unified as Cyclist. The perception range is set to $[-21.0\text{m}, 21.0\text{m}]$ for X and Y axis and $[-2.0\text{m}, 6.0\text{m}]$ for Z axis. There are 573,697 Pedestrian, 43,363 Car, and 8,355 Cyclist labels valid.

Mobile robot: Intelligent wheelchair robot is selected as the mobile robot platform, as shown in Fig. 5, which is equipped with a 16-line LiDAR RS Lidar-16, an RGB-D camera RealSense D435i, a CPU of i5-12400F and a GPU of NVIDIA GeForce RTX 3060.

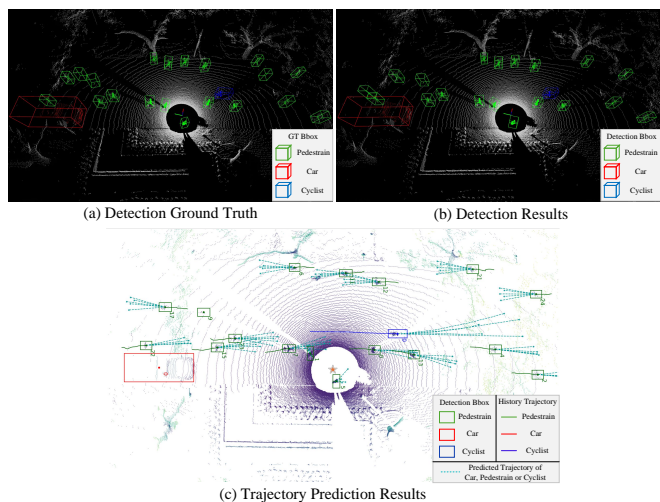


Fig. 6: Visualization of detection and trajectory prediction results of our method for the same frame on CODa. (a) labels the 3D Bboxes of ground truth in the point cloud, while (b) labels the 3D Bboxes of detection. (c) shows the object Bboxes, object IDs, history trajectories, and predicted trajectories with top-5 confidence scores of the tracked objects in BEV.

TABLE II: Performance of tracking models on CODa

Methods	MOTA(Pedestrian)	MOTA(Car)	MOTA(Cyclist)	mMOTA	Infer time
AB3DMOT [39]	0.6166	0.4902	0.4994	0.5354	40.7ms
FastPoly [42]	0.6142	0.4819	0.4906	0.5296	18.4ms
SimpleTrack [11]	0.6232	0.4923	0.5054	0.5403	82.1ms
SimpleTrack*	0.6238	0.4967	0.5042	0.5416	7.4ms

A. Detection Experiment

We use CODa dataset to train and test the detection model CMDT. CMDT uses the pre-trained ResNet50 [52] and a regular VoxelNet [25] as backbones, with 500 queries and truncation thresholds $[0.2, 0.15, 0.1, 0.05, 0, 0]$ for 6 layers of decoder. The model is trained for 30 epochs on 2×3090 GPUs with CBGS strategy training, AdamW optimizer, cosine annealing learning strategy, and learning rate of 3.5×10^{-4} . We terminate the denoising strategy after 20 epochs of training.

We choose CenterPoint [26], BEVFusion [7], and CMT [10] to compare with CMDT, where CMT uses the same backbone and the number of queries as CMDT. The performance of these models on the CODa test set is shown in Table I. The evaluation metric is Average Precision (AP) in BEV view as the same as the KITTI, with IOU thresholds of 0.5, 0.7, and 0.5 for Pedestrian, Car, and Cyclist, and mAP is the mean value of AP for three classes. CMDT outperforms these representative models in all classes. Fig. 6 (a)(b) shows a frame of detection results of CMDT in dynamic scenarios.

B. Tracking Experiment

We choose TBD methods AB3DMOT [39], FastPoly [42], and the original SimpleTrack [11] to compare with the improved SimpleTrack (denoted as SimpleTrack*), and all models take the detection results of the CMDT in IV-A as input.

The performance of these models on the CODa test set is shown in Table II. The evaluation metric is Multiple Object Tracking Accuracy (MOTA) with positive samples calculated in the same way as in IV-A, and mMOTA is the mean value of MOTA for three classes. We also test the inference speed

TABLE III: Performance of trajectory prediction models on CODa. RTMCT(tracking input) means using tracking results as input. Other models use ground truth as input.

Methods	ADE(Pedestrian) _{3/5/10}	ADE(Car) _{3/5/10}	ADE(Cyclist) _{3/5/10}	FDE(Pedestrian) _{3/5/10}	FDE(Car) _{3/5/10}	FDE(Cyclist) _{3/5/10}
Social-GAN [21]	0.2975/0.2791/0.2586	1.1160/1.0673/1.0144	1.6706/1.5358/1.3866	0.5218/0.4821/0.4369	2.0744/1.9656/1.8502	3.2201/2.9324/2.6106
Social-Implicit [20]	0.3532/0.3358/0.3164	0.8158/0.7998/0.7811	1.1291/1.1107/1.0889	0.6175/0.5816/0.5402	1.5213/1.4878/1.4473	2.1216/2.0855/2.0399
RTMCT	0.2667/0.2383/0.2083	0.3894/0.3519/0.3143	0.8490/0.7785/0.7174	0.4664/0.4058/0.3390	0.6977/0.6138/0.5229	1.7548/1.5888/1.4520
RTMCT(tracking input)	0.2466/0.2188/0.1916	0.4172/0.3846/0.3548	0.8572/0.7736/0.7001	0.4308/0.3702/0.3072	0.6848/0.6086/0.5330	1.7488/1.5702/1.4092

TABLE IV: Performance of detection model on wheelchair dataset

Methods	AP(Pedestrian)	AP(Cyclist)	mAP
CMDT	75.15	69.83	72.49

TABLE V: Performance of tracking model on wheelchair dataset

Methods	MOTA(Pedestrian)	MOTA(Cyclist)	mMOTA
SimpleTrack*	0.5915	0.3993	0.4954

of the different models on a platform with an i5-12400F CPU and a 3060 GPU. There is not much difference in accuracy between different models. However, SimpleTrack* can run on GPUs with significantly faster speed than the other models.

C. Trajectory Prediction Experiment

In trajectory prediction experiment, we choose Social-GAN [21] and Social-Implicit [20] to compare with RTMCT. We use labels from the CODa train and test sets as inputs and truth values to train and evaluate these models. For the RTMCT model, we also used the tracking results from CMDT + SimpleTrack* as inputs and labels as truth values to evaluate its performance when actually deployed. Since Social-GAN and Social-Implicit cannot input multiple classes, they do not distinguish classes of trajectories during training and inference.

We set $T_{obs} = 16$, $T_{min} = 2$ and $T_{pred} = 24$. For the RTMCT, the neighbor distance thresholds for Pedestrian, Car, Cyclist and self robots are 2m, 5m, 3m and 2m, the number of reference future trajectories $n = 49$, and the number of decoder layers is 2. It is trained on a 3060 GPU with a CBGS strategy and a learning rate of 1.0×10^4 .

The performance of these models on the CODa test set is shown in Table III. The evaluation metrics are the minimal Average Displacement Error (ADE) and Final Displacement Error (FDE) for predicted trajectory numbers of 3, 5, and 10. When taking the tracking results as input, the negative samples do not have matching truth values, so we only compute metrics for positive samples. Since Social-GAN and Social-Implicit do not distinguish classes, they perform poorly on Car and Cyclist, which have a small number of samples, whereas RTMCT has high accuracy for all classes, regardless of inputs of truth values or tracking results. Fig. 6 (c) shows a frame of prediction results of RTMCT.

D. Experiment on Wheelchair Robot

Compared to the sensors used in CODa, our LiDAR has fewer lines (16 lines compared to 128 lines) and our camera has lower resolution (640×480 compared to 1224×1024). We set perception range to $[0.0m, 15.0m]$ for X and $[-10.0m, 10.0m]$ for Y axis, then collect and annotate 1211 data frames outdoors using the wheelchair robot to form the wheelchair dataset. The dataset has a frame rate of 5 fps with labeled object classes Pedestrian and Cyclist, which has 2600

TABLE VI: Performance of trajectory prediction model on wheelchair dataset

Methods	ADE(Pedestrian) _{3/5/10}	ADE(Cyclist) _{3/5/10}
RTMCT	0.4107/0.3610/0.3242	0.9608/0.8348/0.7362
FDE(Pedestrian) _{3/5/10}		FDE(Cyclist) _{3/5/10}
RTMCT	0.7726/0.6690/0.5870	1.8323/1.5787/1.3629

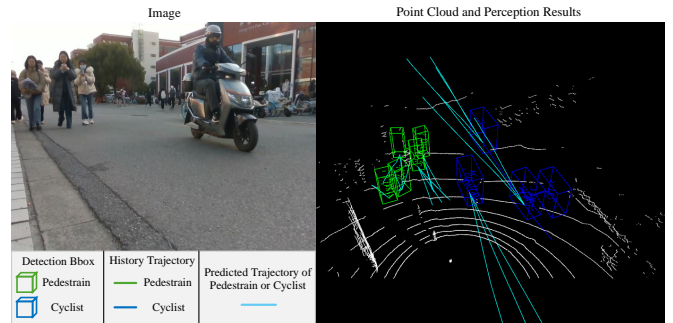


Fig. 7: Detection and trajectory prediction results of our method on the wheelchair robot.

Pedestrian labels and 1302 Cyclist labels, and is split into training and test sets with lengths of 861 and 350.

The wheelchair dataset is too small to directly train the detection model CMDT. Thus, we downsample the point cloud data in CODa collected by 128-line LiDAR to the density of 16-line LiDAR, and set the input image resolution and detection range of CMDT to be the same as the wheelchair dataset, and the number of query is reduced from 500 to 150. The CMDT network parameters CMDT-CODa trained on the original CODa are then used as the initial parameters, and the new model CMDT-CODa* is trained with the modified CODa and network settings by the same training strategies. Finally, CMDT-Wheelchair is trained on the wheelchair dataset using CMDT-CODa* as the initial parameters still by the same training strategies. The performance of CMDT-Wheelchair on the wheelchair test set is shown in Table IV, with detection accuracy comparable to that of CODa test set in IV-A in a smaller perception range.

Taking the detection results of CMDT as input, the performance of the tracking model SimpleTrack* on the wheelchair test set is shown in Table V, which generally meets our requirements.

For the trajectory prediction model, since the frame rate of the wheelchair dataset is 5 fps, reset $T_{obs} = 8$, $T_{pred} = 12$, with other parameters unchanged. RTMCT can be trained directly on the wheelchair training set of small samples, and its performance on the wheelchair test set is shown in Table VI. Due to less training data, the accuracy is a little worse than in IV-C, but it also generally meets our requirements.

We deploy the model on the wheelchair robot platform and

run it in the campus environment, as shown in Fig. 7. Its inference speed is shown in Table VII, which can reach 13.2 fps and fully meets the real-time demand. In addition, A video submitted with the paper shows the real-time inference results of our method on the wheelchair robot in both indoor and outdoor environments.

TABLE VII: Inference time of our method on the wheelchair

Task	Detection	Tracking	Trajectory Prediction	Total
Inference Time	64.7 ms	8.0 ms	2.9 ms	75.6 ms

TABLE VIII: Comparison of different cross attention in CMDT

Cross Attention	AP(Pedestrian)	AP(Car)	AP(Cyclist)	mAP	GPU Memory
Regular Attention	80.91	62.84	66.91	70.22	172.2MB
MMDA	81.15	65.24	69.38	71.92	38.9MB

TABLE IX: Comparison of different training strategies used in CMDT. Truncated Loss means using 3D box truncation L1 loss. Early Stop DN means stopping denoising strategy early.

Truncated Loss	Early Stop DN	AP(Pedestrian)	AP(Car)	AP(Cyclist)	mAP
×	×	80.95	64.23	68.35	71.18
✓	×	81.10	64.96	69.01	71.69
×	✓	81.03	64.77	68.69	71.50
✓	✓	81.15	65.24	69.38	71.92

E. Ablation Study

1) *Detection Model*: In order to analyze the performance of the MMDA module, we choose regular global attention and MMDA as cross-attention of CMDT. Their performances on the CODa test set are shown in Table VIII, which shows that MMDA outperforms the regular global attention in both accuracy and memory usage.

We improve the training strategies of CMDT, including the 3D bounding box truncated L1 loss and early termination of denoising strategies. On the CODa test set, the effects of these strategies on the model are shown in Table IX. It can be seen that using one of the strategies outperforms not using strategies, while using both performs best, showing that the improvements for training strategies are effective.

2) *Trajectory Prediction Model*: RTMCT uses a 2-layer decoder, we try to change the number of decoder layers to 1 or 3. Their performances on the CODa test set are shown in Table X, which shows that the accuracy of 1-layer and 3-layer cases is worse than the 2-layer case.

In RTMCT, different classes of objects are encoded and output using different linear layers while sharing the transformer. We try to make different classes of objects share all networks including linear layers and the transformer (named Share All), or not to share any networks (named No Share). Their performances on the CODa test set are shown in Table XI, which shows that their average accuracy is also worse than the original model.

V. CONCLUSION

In this paper, we propose the detection model CMDT improves the accuracy of object detection, and the trajectory prediction model RTMCT achieves flexible length trajectory prediction for multi-class objects while reducing trajectory

TABLE X: Comparison of different numbers of decoder layers in RTMCT

Decoder Layer Num	ADE(Pedestrian) _{3/5/10}	ADE(Car) _{3/5/10}	ADE(Cyclist) _{3/5/10}
1	0.2687/0.2401/0.2093	0.4025/0.3636/0.3161	0.8690/0.8003/0.7394
2	0.2667/0.2383/0.2083	0.3894/0.3519/0.3143	0.8490/0.7785/0.7174
3	0.3047/0.2864/0.2622	0.4045/0.3668/0.3300	0.8430/0.7756/0.7086

Decoder Layer Num	FDE(Pedestrian) _{3/5/10}	FDE(Car) _{3/5/10}	FDE(Cyclist) _{3/5/10}
1	0.4731/0.4062/0.3398	0.7385/0.6460/0.5320	1.7903/1.6449/1.5033
2	0.4664/0.4058/0.3390	0.6977/0.6138/0.5229	1.7548/1.5888/1.4520
3	0.5489/0.5113/0.4606	0.7391/0.6505/0.5565	1.7373/1.5846/1.4325

TABLE XI: Comparison of different choices of shared network in RTMCT

Network Type	ADE(Pedestrian) _{3/5/10}	ADE(Car) _{3/5/10}	ADE(Cyclist) _{3/5/10}
Share All	0.2686/0.2398/0.2085	0.4468/0.4137/0.3764	0.8214/0.7559/0.6835
No Share	0.2629/0.2323/0.2013	0.3954/0.3665/0.3285	0.8964/0.8401/0.7864
Original Network	0.2667/0.2383/0.2083	0.3894/0.3519/0.3143	0.8490/0.7785/0.7174

Network Type	FDE(Pedestrian) _{3/5/10}	FDE(Car) _{3/5/10}	FDE(Cyclist) _{3/5/10}
Share All	0.4691/0.4083/0.3407	0.8121/0.7365/0.6496	1.7199/1.5317/1.4135
No Share	0.4586/0.3966/0.3309	0.7030/0.6355/0.5444	1.8365/1.7157/1.5977
Original Network	0.4664/0.4058/0.3390	0.6977/0.6138/0.5229	1.7548/1.5888/1.4520

prediction errors. Then we develop an algorithm for service mobile robots to detect, track, and predict trajectories for objects such as pedestrians, vehicles, and riders. On the dataset CODa, our method outperforms many representative methods. With little training data, we apply the method to a wheelchair robot and achieve an inference speed of 13.2fps.

However, there is still some space for improvement. Our detection model only utilize single frame of sensor information, and trajectory prediction model only utilize observed trajectories without considering environmental information. We can improve the detection performance by using the feature map or object query features of the previous frames, and reduce the trajectory prediction error by using geometric or semantic map. Despite the robustness of the LiDAR-camera fusion method, we don't train and test the model for some special scenarios, such as scenes with fast-moving objects and nighttime scenes. These issues will be addressed in our future work.

ACKNOWLEDGMENT

This work is supported by the National Key R&D Program of China (Grant 2020YFC2007500), and the Science and Technology Commission of Shanghai Municipality (Grant 20DZ2220400).

REFERENCES

- [1] T. Deng, G. Shen, T. Qin, *et al.*, "Pigslam: Progressive neural scene representation with local to global bundle adjustment," in *Proceedings of the IEEE/CVF Conference on Computer Vision and Pattern Recognition (CVPR)*, June 2024, pp. 19 657–19 666.
- [2] T. Deng, Y. Wang, H. Xie, *et al.*, "Neslam: Neural implicit mapping and self-supervised feature tracking with depth completion and denoising," *IEEE Transactions on Automation Science and Engineering*, pp. 1–1, 2025.
- [3] L. Chen, P. Wu, K. Chitta, *et al.*, "End-to-end autonomous driving: Challenges and frontiers," *IEEE Transactions on Pattern Analysis and Machine Intelligence*, vol. 46, no. 12, pp. 10 164–10 183, 2024.
- [4] Y. Hu, J. Yang, L. Chen, *et al.*, "Planning-oriented autonomous driving," in *IEEE/CVF Conference on Computer Vision and Pattern Recognition (CVPR)*, 2023, pp. 17 853–17 862.
- [5] S. Vora, A. H. Lang, B. Helou, *et al.*, "Pointpainting: Sequential fusion for 3d object detection," in *IEEE/CVF Conference on Computer Vision and Pattern Recognition (CVPR)*, 2020, pp. 4603–4611.
- [6] H. Wu, C. Wen, S. Shi, *et al.*, "Virtual sparse convolution for multimodal 3d object detection," in *IEEE/CVF Conference on Computer Vision and Pattern Recognition (CVPR)*, 2023, pp. 21 653–21 662.

- [7] Z. Liu, H. Tang, A. Amini, *et al.*, “Bevfusion: Multi-task multi-sensor fusion with unified bird’s-eye view representation,” in *2023 IEEE International Conference on Robotics and Automation (ICRA)*, 2023, pp. 2774–2781.
- [8] Y. Wang, V. C. Guizilini, T. Zhang, *et al.*, “Detr3d: 3d object detection from multi-view images via 3d-to-2d queries,” in *Conference on Robot Learning (CORL)*, 2022, pp. 180–191.
- [9] Y. Liu, T. Wang, X. Zhang, *et al.*, “Petr: Position embedding transformation for multi-view 3d object detection,” in *European conference on computer vision (ECCV)*, 2022, pp. 531–548.
- [10] J. Yan, Y. Liu, J. Sun, *et al.*, “Cross modal transformer: Towards fast and robust 3d object detection,” in *2023 IEEE/CVF International Conference on Computer Vision (ICCV)*, 2023, pp. 18 222–18 232.
- [11] Z. Pang, Z. Li, and N. Wang, “Simpletrack: Understanding and rethinking 3d multi-object tracking,” in *European conference on computer vision (ECCV)*, 2022, pp. 680–696.
- [12] J. Gao, C. Sun, H. Zhao, *et al.*, “Vectornet: Encoding hd maps and agent dynamics from vectorized representation,” in *IEEE Conference on Computer Vision and Pattern Recognition (CVPR)*, 2020, pp. 11 525–11 533.
- [13] R. Greer, N. Deo, and M. Trivedi, “Trajectory prediction in autonomous driving with a lane heading auxiliary loss,” *IEEE Robotics and Automation Letters*, vol. 6, no. 3, pp. 4907–4914, 2021.
- [14] L. Zhang, P. Li, S. Liu, *et al.*, “Simpl: A simple and efficient multi-agent motion prediction baseline for autonomous driving,” *IEEE Robotics and Automation Letters*, 2024.
- [15] A. Alahi, K. Goel, V. Ramanathan, *et al.*, “Social lstm: Human trajectory prediction in crowded spaces,” in *IEEE Conference on Computer Vision and Pattern Recognition (CVPR)*, 2016, pp. 961–971.
- [16] Y. Huang, H. Bi, Z. Li, *et al.*, “Stgat: Modeling spatial-temporal interactions for human trajectory prediction,” in *2019 IEEE/CVF International Conference on Computer Vision (ICCV)*, 2019, pp. 6271–6280.
- [17] C. Yu, X. Ma, J. Ren, *et al.*, “Spatio-temporal graph transformer networks for pedestrian trajectory prediction,” in *European conference on computer vision (ECCV)*, 2020, pp. 507–523.
- [18] N. Lee, W. Choi, P. Vernaza, *et al.*, “Desire: Distant future prediction in dynamic scenes with interacting agents,” in *IEEE Conference on Computer Vision and Pattern Recognition (CVPR)*, 2017, pp. 2165–2174.
- [19] P. Xu, J.-B. Hayet, and I. Karamouzas, “Socialvae: Human trajectory prediction using timewise latents,” in *European Conference on Computer Vision (ECCV)*, 2022, pp. 511–528.
- [20] A. Mohamed, D. Zhu, W. Vu, *et al.*, “Social-implicit: Rethinking trajectory prediction evaluation and the effectiveness of implicit maximum likelihood estimation,” in *European Conference on Computer Vision (ECCV)*, 2022, pp. 463–479.
- [21] A. Gupta, J. Johnson, L. Fei-Fei, *et al.*, “Social gan: Socially acceptable trajectories with generative adversarial networks,” in *IEEE/CVF Conference on Computer Vision and Pattern Recognition (CVPR)*, 2018, pp. 2255–2264.
- [22] A. Sadeghian, V. Kosaraju, A. Sadeghian, *et al.*, “Sophie: An attentive gan for predicting paths compliant to social and physical constraints,” in *IEEE/CVF Conference on Computer Vision and Pattern Recognition (CVPR)*, 2019, pp. 1349–1358.
- [23] A. Zhang, C. Eranki, C. Zhang, *et al.*, “Toward robust robot 3-d perception in urban environments: The ut campus object dataset,” *IEEE Transactions on Robotics*, vol. 40, pp. 3322–3340, 2024.
- [24] Y. Zhou and O. Tuzel, “Voxelnet: End-to-end learning for point cloud based 3d object detection,” in *IEEE/CVF Conference on Computer Vision and Pattern Recognition (CVPR)*, June 2018.
- [25] Y. Yan, Y. Mao, and B. Li, “Second: Sparsely embedded convolutional detection,” *Sensors*, vol. 18, no. 10, p. 3337, 2018.
- [26] T. Yin, X. Zhou, and P. Krähenbühl, “Center-based 3d object detection and tracking,” in *IEEE/CVF Conference on Computer Vision and Pattern Recognition (CVPR)*, 2021, pp. 11 779–11 788.
- [27] Y. Yuan, H. Cheng, and M. Sester, “Keypoints-based deep feature fusion for cooperative vehicle detection of autonomous driving,” *IEEE Robotics and Automation Letters*, vol. 7, no. 2, pp. 3054–3061, 2022.
- [28] J. Philion and S. Fidler, “Lift, splat, shoot: Encoding images from arbitrary camera rigs by implicitly unprojecting to 3d,” in *European conference on computer vision (ECCV)*, 2020, pp. 194–210.
- [29] C. Reading, A. Harakeh, J. Chae, *et al.*, “Categorical depth distribution network for monocular 3d object detection,” in *IEEE/CVF Conference on Computer Vision and Pattern Recognition (CVPR)*, 2021, pp. 8551–8560.
- [30] J. Huang, G. Huang, Z. Zhu, *et al.*, “Bevdet: High-performance multi-camera 3d object detection in bird-eye-view,” *arXiv preprint arXiv:2112.11790*, 2021.
- [31] Z. Li, Z. Ge, G. Yu, *et al.*, “Bevformer: Learning bird’s-eye-view representation from lidar-camera via spatiotemporal transformers,” *IEEE Transactions on Pattern Analysis and Machine Intelligence*, vol. 47, no. 3, pp. 2020–2036, 2025.
- [32] Y. Li, Z. Ge, G. Yu, *et al.*, “Bevdepth: Acquisition of reliable depth for multi-view 3d object detection,” in *Proceedings of the AAAI conference on artificial intelligence*, vol. 37, no. 2, 2023, pp. 1477–1485.
- [33] N. Carion, F. Massa, G. Synnaeve, *et al.*, “End-to-end object detection with transformers,” in *European conference on computer vision (ECCV)*, 2020, pp. 213–229.
- [34] X. Zhu, W. Su, L. Lu, *et al.*, “Deformable detr: Deformable transformers for end-to-end object detection,” *arXiv preprint arXiv:2010.04159*, 2020.
- [35] F. Li, H. Zhang, S. Liu, *et al.*, “Dn-detr: Accelerate detr training by introducing query denoising,” *IEEE Transactions on Pattern Analysis and Machine Intelligence*, vol. 46, no. 4, pp. 2239–2251, 2024.
- [36] H. Zhang, F. Li, S. Liu, *et al.*, “Dino: Detr with improved denoising anchor boxes for end-to-end object detection,” *arXiv preprint arXiv:2203.03605*, 2022.
- [37] V. A. Sindagi, Y. Zhou, and O. Tuzel, “Mvx-net: Multimodal voxelnet for 3d object detection,” in *2019 International Conference on Robotics and Automation (ICRA)*, 2019, pp. 7276–7282.
- [38] A. Bewley, Z. Ge, L. Ott, *et al.*, “Simple online and realtime tracking,” in *2016 IEEE International Conference on Image Processing (ICIP)*, 2016, pp. 3464–3468.
- [39] X. Weng, J. Wang, D. Held, *et al.*, “Ab3dmot: A baseline for 3d multi-object tracking and new evaluation metrics,” *arXiv preprint arXiv:2008.08063*, 2020.
- [40] L. Wang, X. Zhang, W. Qin, *et al.*, “Camo-mot: Combined appearance-motion optimization for 3d multi-object tracking with camera-lidar fusion,” *IEEE Transactions on Intelligent Transportation Systems*, vol. 24, no. 11, pp. 11 981–11 996, 2023.
- [41] X. Wang, C. Fu, J. He, *et al.*, “A multi-modal fusion-based 3d multi-object tracking framework with joint detection,” *IEEE Robotics and Automation Letters*, 2024.
- [42] X. Li, D. Liu, Y. Wu, *et al.*, “Fast-poly: A fast polyhedral algorithm for 3d multi-object tracking,” *IEEE Robotics and Automation Letters*, 2024.
- [43] X. Zhou, V. Koltun, and P. Krähenbühl, “Tracking objects as points,” in *European conference on computer vision (ECCV)*, 2020, pp. 474–490.
- [44] J. Peng, C. Wang, F. Wan, *et al.*, “Chained-tracker: Chaining paired attentive regression results for end-to-end joint multiple-object detection and tracking,” in *European conference on computer vision (ECCV)*, 2020, pp. 145–161.
- [45] P. Sun, J. Cao, Y. Jiang, *et al.*, “Transtrack: Multiple object tracking with transformer,” *arXiv preprint arXiv:2012.15460*, 2020.
- [46] T. Meinhardt, A. Kirillov, L. Leal-Taixé, *et al.*, “Trackformer: Multi-object tracking with transformers,” in *IEEE/CVF Conference on Computer Vision and Pattern Recognition (CVPR)*, 2022, pp. 8834–8844.
- [47] Y. Xu, Y. Ban, G. Delorme, *et al.*, “Transcenter: Transformers with dense representations for multiple-object tracking,” *IEEE Transactions on Pattern Analysis and Machine Intelligence*, vol. 45, no. 6, pp. 7820–7835, 2023.
- [48] T. Zhang, X. Chen, Y. Wang, *et al.*, “Mutr3d: A multi-camera tracking framework via 3d-to-2d queries,” in *Proceedings of the IEEE/CVF Conference on Computer Vision and Pattern Recognition*, 2022, pp. 4537–4546.
- [49] Z. Pang, J. Li, P. Tokmakov, *et al.*, “Standing between past and future: Spatio-temporal modeling for multi-camera 3d multi-object tracking,” in *IEEE/CVF Conference on Computer Vision and Pattern Recognition (CVPR)*, 2023, pp. 17 928–17 938.
- [50] S. Ding, L. Schneider, M. Cordts, *et al.*, “Ada-track: End-to-end multi-camera 3d multi-object tracking with alternating detection and association,” in *Proceedings of the IEEE/CVF Conference on Computer Vision and Pattern Recognition*, 2024, pp. 15 184–15 194.
- [51] A. Geiger, P. Lenz, and R. Urtasun, “Are we ready for autonomous driving? the kitti vision benchmark suite,” in *IEEE/CVF Conference on Computer Vision and Pattern Recognition (CVPR)*, 2012, pp. 3354–3361.
- [52] K. He, X. Zhang, S. Ren, *et al.*, “Deep residual learning for image recognition,” in *IEEE/CVF Conference on Computer Vision and Pattern Recognition (CVPR)*, June 2016.